Journal of Magnetic Resonance 205 (2010) 242–246

Contents lists available at ScienceDirect

Journal of Magnetic Resonance

journal homepage: www.elsevier.com/locate/jmr

Xenon-based molecular sensors in lipid suspensions

Tyler Meldrum [a,c], Leif Schröder [a,c,1], Philipp Denger [d], David E. Wemmer [b,c], Alexander Pines [a,c,*]

[a] Materials Sciences Division, Lawrence Berkeley National Laboratory, Berkeley, CA 94720, USA
[b] Physical Biosciences Division, Lawrence Berkeley National Laboratory, Berkeley, CA 94720, USA
[c] Department of Chemistry, University of California, Berkeley, CA 94720, USA
[d] Abtlg. Medizinische Physik in der Radiologie (Division of Medical Physics in Radiology), Deutsches Krebsforschungszentrum, Im Neuenheimer Feld 280, 69120 Heidelberg, Germany

ARTICLE INFO

Article history:
Received 9 March 2010
Revised 7 May 2010
Available online 13 May 2010

Keywords:
Biosensors
Cryptophane
Host–guest systems
Lipid vesicles
Xenon

ABSTRACT

There have been many proposals to use xenon-based molecular sensors in biological settings. Fundamental to understanding the properties of these sensors *in vivo* is characterizing their behavior in lipid environments. We report the investigation of xenon-based molecular sensors in suspensions of lipid vesicles with a size comparable to cells. We detail spectroscopic properties of sensors associated with lipid vesicles as well as those in equilibrium in the surrounding solution. We characterize the dependence of the spectral parameters on temperature, relevant for studies at physiological temperatures. We also demonstrate the ability to perform selective saturation transfer (Hyper-CEST) between sensor, both lipid bound and unbound, and the bulk solution. Lastly, we demonstrate the applicability of saturation transfer in the heterogeneous medium as an imaging modality.

1. Introduction

Xenon-based molecular sensors are host molecules that are designed to give a unique magnetic resonance (MR) signal from a xenon atom that is temporarily encapsulated [1]. These sensors, often referred to as xenon biosensors, can be conjugated with a moiety that confers chemical specificity for binding to a particular analyte; examples of such binding moieties are biotin or avidin [1], oligonucleotides or aptamers [2,3], or enzyme substrates [4]. Binding to a molecular target causes localization of the sensor in regions containing the analyte, making it possible to image the target of chemical interest [5]. While there is great potential in using these sensors for targeted molecular imaging *in vivo*, for example, in the determination of distributions of cell surface receptors [3], their non-specific interactions with many biological materials are poorly understood. Some interaction between the hydrophobic xenon-binding moiety (a cryptophane molecule) that has been targeted to a cell surface receptor and the hydrophobic interior of the cell membrane is likely. Studies have been conducted on cryptophanes in hydrophobic organic solvents [6,7] and in human plasma [8], but there has been no previous report on the interaction of cryptophanes with lipid vesicles.

We investigated interactions between cryptophane and lipid vesicles that are comparable in size and composition to cell membranes [9] using xenon NMR; the system is shown schematically in Fig. 1. Lipid vesicles have been successfully used as carrier agents for xenon (without cryptophane-based sensors) in MR angiography [9] and in MR imaging of the rat brain [10]; these and other reports [11,12] indicate that xenon is more soluble in lipids than in water. In addition, we hypothesized that cryptophane, a hydrophobic molecule, would show greater solubility in a lipid emulsion than in pure water. The increased solubility of both xenon and the sensor is advantageous in maximizing signal. Furthermore, we hoped to resolve the signals corresponding to free xenon dissolved in both aqueous and lipid environments, as well as the signals corresponding to xenon bound in the sensor in both aqueous and lipid environments. We wanted to extend previous work involving the temperature dependence of the chemical shift values for these signals. Lastly, we predicted that we could selectively image the sensor in aqueous and lipid environments, illustrating the application of xenon-based molecular sensors to targeted imaging in biological mixtures.

2. Results and discussion

2.1. Lipid suspensions vs. aqueous solutions

In all experiments reported here, we used a variant of cryptophane-A cage (inset in Fig. 1) as a xenon host. This cage molecule has acetate groups chemically attached to its exterior, conferring partial solubility in the aqueous phase of the suspension; we refer

* Corresponding author at: Materials Sciences Division, Lawrence Berkeley National Laboratory, Berkeley, CA 94720, USA. Fax: +1 510 666 3768.
E-mail address: pines@berkeley.edu (A. Pines).
[1] Present address: Molecular Imaging Group, Leibniz-Institut für Molekulare Pharmakologie, Robert-Rössle-Str. 10, 13125 Berlin, Germany.

1090-7807/$ - see front matter © 2010 Elsevier Inc. All rights reserved.
doi:10.1016/j.jmr.2010.05.005

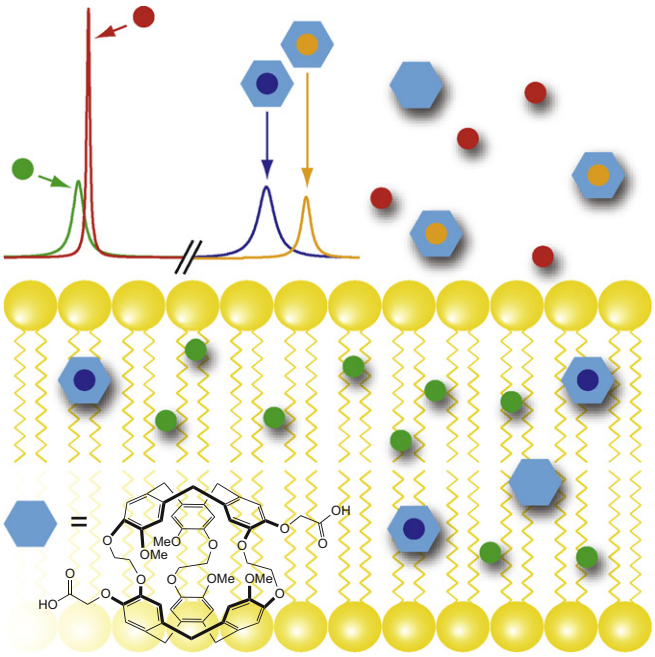

Fig. 1. A schematic of the various pools of xenon in this study. Xe_{lipid} (green) and Xe_{aq} (red) correspond to unbound xenon. $Xe@cage_{lipid}$ (dark blue) and $Xe@cage_{aq}$ (yellow) appear ~130 ppm upfield of the Xe_{aq} peak. The cage is represented by the light blue hexagon. The modified cryptophane cage used in these studies, shown in the inset, is termed "diacid cage". The introduction of two acetate groups confers some water solubility to this otherwise hydrophobic molecule.

to this cryptophane compound as diacid cage. A saturated aqueous solution has 15 ± 5 μM of the diacid cage, as determined by UV–vis absorbance (ε_{287nm} = 8000 M^{-1} cm^{-1}) [13].

The NMR spectrum of xenon bubbled into pure water shows peaks corresponding to gaseous xenon (referenced to 0 ppm) and to xenon dissolved in water (Xe_{aq}) at 189 ppm. Fig. 2 shows the xenon-NMR spectrum of diacid cage in water (black), with resonances at 62 and 189 ppm, corresponding to xenon bound in the cryptophane cage in an aqueous environment ($Xe@cage_{aq}$) and free

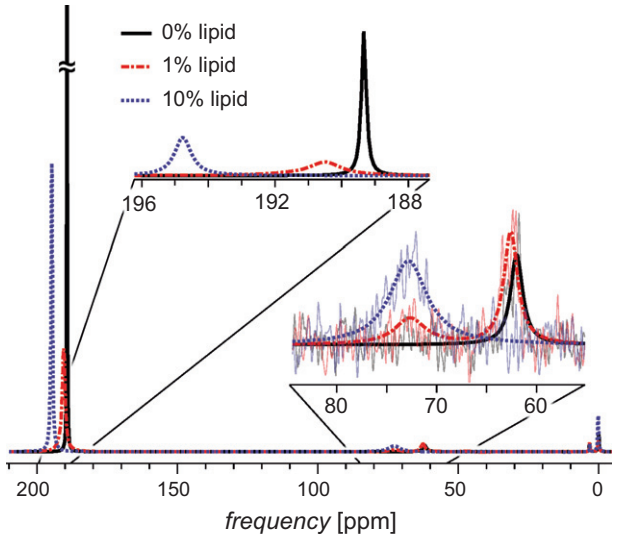

Fig. 2. Xenon NMR spectra of the diacid cage in samples of 0% (black), 1% (red), and 10% (blue) lipid content. The peaks at ~190 ppm correspond to the Xe_{aq} and Xe_{lipid} peaks, while the peaks at 63 and 73 ppm correspond to $Xe@cage_{aq}$ and $Xe@cage_{lipid}$, respectively. (For interpretation of the references to color in this figure legend, the reader is referred to the web version of this article.)

xenon in aqueous solution (Xe_{aq}), respectively. These shifts are consistent with those reported elsewhere [1].

The spectrum of diacid cryptophane in a 1% lipid suspension (red in Fig. 2) showed three resonances: the two found in the pure aqueous solution and a third resonance at 73 ppm. We attribute this third resonance to that of xenon bound in the cryptophane cage in a lipid environment ($Xe@cage_{lipid}$). The integrated areas of the Xe@cage peaks in the 1% lipid suspension give relative signal intensities of 1:2 ($Xe@cage_{lipid}$:$Xe@cage_{aq}$). Because this ratio is much larger than the lipid/water volume ratio (1:100), we estimate that diacid cage is at least 50 times more soluble in lipid than in water. As previous data show that the binding affinity of xenon for the cage in water is greater than in an apolar solvent [14], it is unlikely that the 1:2 ratio of the $Xe@cage_{lipid}$:$Xe@cage_{aq}$ signals can be explained by a greater fraction of cages containing xenon in the lipid phase. With 5% and 2% lipid suspensions, both $Xe@cage_{aq}$ and the $Xe@cage_{lipid}$ peaks were clearly visible, but when the lipid content was increased to 10%, only one peak was observed: $Xe@cage_{lipid}$ at 73 ppm (blue in Fig. 2). The ratio of peak intensities, $Xe@cage_{lipid}$:$Xe@cage_{aq}$, for the 2% and 5% lipid suspensions was 0.9:1 and 1.6:1, respectively. This increase of the $Xe@cage_{lipid}$:$Xe@cage_{aq}$ ratio with lipid content verifies the preferential partitioning of cage and xenon into the aliphatic lipid environment.

Beyond the changes in the Xe@cage peaks due to lipid content, we note that the peak at 189 ppm shifts downfield and is broadened upon addition of the lipid. We fitted this region of the spectrum using two Lorentzian curves, representing the Xe_{aq} and Xe_{lipid} peaks. These fits show a broad peak ~1 ppm downfield of a narrower, more intense peak. We attribute the more intense peak to Xe_{aq} because it has a chemical shift value closer to that of Xe_{aq} from the 0% lipid solution. The chemical shift value for the Xe_{aq} peak increases with increasing lipid content; this effect, reported previously with proteins [15], is a result of weak surface interactions between xenon atoms and other molecules in solution. The observation of distinct Xe_{aq} and Xe_{lipid} peaks indicates that these two pools exchange slowly on the chemical shift timescale. While the integrated areas of the solvent peaks do not show a quantitative relationship with the lipid content of a given sample, a trend of increasing Xe_{lipid} peak area with increasing lipid content is observed. The lack of quantitative agreement is probably due to error in the fits resulting from the large difference in the intensities of the two fitted peaks. Nevertheless, the fit parameters yield a systematic trend for the chemical shift values of both the Xe_{aq} and Xe_{lipid} peaks, supporting the validity of the fits, which are provided as Supporting Information. Interestingly, we note that the chemical shift separation between the xenon signals in aqueous and lipid environments without the cage (~1 ppm) is ten times smaller than the separation with the cage (~10 ppm). This ability of a host molecule to amplify the chemical shift separation may be useful in determining the local chemical environment of the cage and other molecules to which the cage may be bound.

2.2. Temperature dependence

We explored the temperature dependence of xenon-based molecular sensors in lipid suspensions at temperatures from 5 °C to 40 °C. Following initial equilibration at room temperature, samples were allowed to equilibrate for 5 min. at each temperature point before data acquisition. At temperatures below 25 °C, the Xe_{lipid} peaks for the 1%, 2%, and 5% lipid suspensions were distinguishable from the Xe_{aq} peaks, as shown in Fig. S2. However, at temperatures above 25 °C the peaks overlapped and could not be fitted unambiguously. Generally, the position of the Xe_{aq} peak varied quadratically with temperature, as has been reported previously [16], while the position of the Xe_{lipid} peak decreased with increasing temperature. The chemical shift values of the $Xe@cage_{aq}$

and Xe@cage$_{lipid}$ peaks showed a linear increase with temperature—the slope of the Xe@cage$_{aq}$ shift was consistent with previous results at 0.31 ± 0.01 ppm °C^{-1} [17], and that of the Xe@cage$_{lipid}$ peak was 0.18 ± 0.03 ppm °C^{-1}. Plots of chemical shift values at different temperatures are available as Supporting Information.

2.3. Saturation transfer

When using xenon-based molecular sensors in mixed aqueous/lipid environments, exchange among four distinct xenon pools affects the system, illustrated schematically in Fig. 1. To qualitatively characterize these exchange pathways between the different pools, we used the approach termed Hyper-CEST [18], analogous to Xenon Polarization Transfer Contrast (XTC) [19], in which a decrease in the Xe$_{aq}$ signal following saturation at the Xe@cage frequency occurs in the presence of the molecular sensor. In our experiments, saturation pulses were 500 ms in duration, much longer than the 30 ms residence time of xenon atoms reported for cryptophane cage in water [13], and were designed to have a bandwidth of ~1.8 ppm (150 Hz) [20].

As shown in Fig. 3, when a saturation pulse was applied at a frequency far off resonance from the Xe@cage signals (spectrum f), no change was observed in the signal intensity of any peak. When the pulse was applied at frequencies at or near the Xe@cage peaks, saturation was observed to varying degrees in other peaks. The results of these saturation transfer experiments are summarized in Table 1. The transfer of saturation between the lipid and aqueous pools indicates chemical exchange of xenon between these two environments on the time scale of the applied saturation pulse (500 ms). The difference in the degree of saturation as a result of pulses applied at the Xe@cage$_{aq}$ vs. Xe@cage$_{lipid}$ frequencies indicates more rapid exchange of xenon in and out of the cage in the lipid phase than in water. This observation is consistent with the linewidths of the Xe@cage peaks; the linewidth of the Xe@cage$_{lipid}$ peak, a property indicative of the exchange rate, is two to five times wider than that of the Xe@cage$_{aq}$ peak in both the 1% and 2% lipid samples (see Supporting Information). Ultimately, higher concentrations of both xenon and cage in the lipid environment, together with more rapid exchange, result in more efficient Hyper-CEST saturation in lipid environments using xenon-based molecular sensors. This increased saturation efficiency could be used to improve xenon NMR detection sensitivity in lipophilic systems.

Table 1
Integrated peak areas of a xenon-NMR spectrum of a 1% lipid suspension following saturation at various frequencies. Letters designating the saturation frequency correspond to the spectra in Fig. 3.

Saturation frequency	Xe$_{lipid}$	Xe$_{aq}$	Xe@cage$_{lipid}$	Xe@cage$_{aq}$
a (−432.8 ppm)	1.00[a]	0.93	0.36	0.18
b (49.7 ppm)	0.82	0.81	0.39	0.15
c (59.4 ppm)[c]	0.58	0.05	0.11	0.09
d (64.3 ppm)	0.40	0.37	0.21	0.06
e (69.1 ppm)[d]	0.10	0.05	0.00[b]	0.00[b]
f (88.6 ppm)	0.82	0.65	0.32	0.14

[a] All peak areas normalized to this value.
[b] No observable peak at this frequency.
[c] This frequency corresponds to Xe@cage$_{aq}$.
[d] This frequency corresponds to Xe@cage$_{lipid}$.

2.4. Imaging

To demonstrate the applicability of frequency-selective Hyper-CEST detection to imaging, we combined saturation with phase-encoded imaging, as shown in Fig. 4. When weak saturation pulses were applied resonant with either Xe@cage$_{lipid}$ or Xe@cage$_{aq}$, the response was total saturation of the Xe$_{aq}$ and Xe$_{lipid}$ peaks, verifying the presence of diacid cage (Fig. 4a and c). In contrast, when saturation was applied at a frequency directly between those of the two cage peaks, insufficient contrast was generated to verify

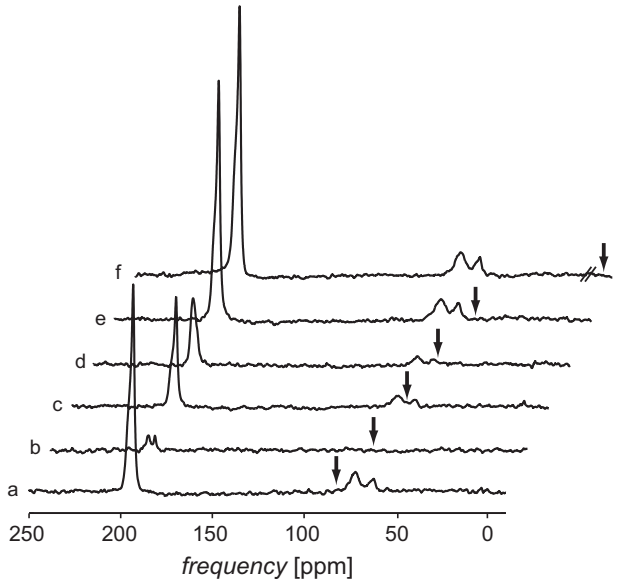

Fig. 3. The xenon NMR spectra following Hyper-CEST saturation at different saturation frequencies as indicated by the small arrows. Saturation is most apparent when saturating directly on the Xe@cage peaks (spectra b and d), especially the Xe@cage$_{lipid}$ peak. When saturating the Xe@cage$_{lipid}$ peak (spectrum b), the individual Xe$_{aq}$ and Xe$_{lipid}$ peaks become apparent due to the reduction in peak intensity.

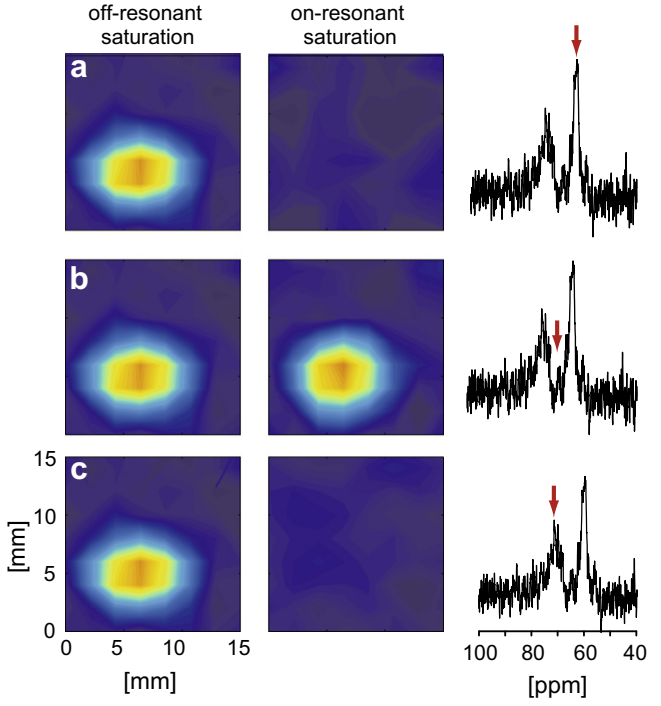

Fig. 4. A demonstration of the selectivity of Hyper-CEST for imaging with the diacid cage in lipid suspension. When saturation is applied to either the Xe@cage$_{aq}$ (a) or Xe@cage$_{lipid}$ (c) peak, the response is diminished in the on-resonant case. When saturation is applied at a frequency between the two Xe@cage peaks (b), there is no apparent saturation in the image. The applied radio frequency field in these imaging experiments is approximately one-fifth the amplitude of that used in Fig. 3, giving increased selectivity.

the presence of cage in the Hyper-CEST images (Fig. 4b). This demonstrates the utility of frequency-selective saturation for detecting multiple molecular sensors with small frequency separations. Based on the unique response of the $Xe@cage_{aq}$ and $Xe@cage_{lipid}$ signals to saturation, we anticipate the development of multiplexing using xenon-based molecular sensors. Incorporating multiplexing with previously reported work on the detection of low concentrations of sensor [17] may provide a facile way to characterize an analyte with NMR in a way analogous to multiplexed optical detection using fluorophores.

3. Conclusion

The NMR signal enhancement resulting from increased amounts of xenon and sensor in lipid environments reduces sensitivity requirements for detection of analytes typically found in lipophilic media. The response of the Xe_{aq} and Xe_{lipid} peaks to saturation at frequencies corresponding to $Xe@cage_{aq}$ and $Xe@cage_{lipid}$ reduces these sensitivity requirements even further. In addition, differences in the chemical shift of xenon in the presence of molecular sensor facilitate the discrimination of the chemical environment of xenon, either aqueous or lipid, with greater frequency resolution than in the absence of sensor. Interestingly, xenon-based molecular sensors in lipid emulsions show a quantitative dependence on temperature; it is possible that a similar dependence on other solvent properties, for example, pH, will emerge in future experiments. By exploiting the response to both magnetization transfer and to physical and chemical properties of the local environment, sensors could be designed that simultaneously analyze several properties of a system of interest, for example, biological or other chemical markers, that appear in different concentrations in lipophilic and hydrophilic regions of the body.

4. Experimental

Dilute suspensions of lipid vesicles were prepared from a pharmaceutical grade lipid suspension (Intralipid® 20%, Pharmacia) that contains vesicles 100–500 nm in diameter [10]. Lipid emulsion was diluted with water/D_2O (minimum 30% D_2O for frequency locking in the spectrometer) to 1%, 2%, 5%, and 10% lipid content. To each aliquot of this dilute lipid suspension (4.0 mL) was added a variant of cryptophane-A (2.0 ± 0.4 mg), termed diacid cage, with two methoxy groups each replaced by methyl carboxylic acid groups for increased water solubility. The concentration of diacid cage in the lipid suspension could not be directly measured during sample preparation because the lipid vesicles strongly scatter light. By allowing the sample to settle for ~10 min after shaking and by pipetting from the top of the suspension, we avoided introducing powder into the NMR sample tubes; thus, the amount of dissolved cage was fixed for any given lipid concentration.

Data were recorded on a 7.05 T NMR spectrometer (Varian, Palo Alto, CA) using 5 mm and 10 mm (spectroscopy) and 30 mm (imaging) probes. Hyperpolarized xenon ($P \approx 4\%$) [21,22] was generated with a XenoSpin polarizer (Amersham Health, Durham, NC) from a gas mixture of 89% He, 10% N_2, and 1% xenon with natural-abundance isotopes (Praxair) at ~70 psi. Gas containing hyperpolarized xenon was bubbled (15–20 s, 0.45 standard liters per minute) into the NMR tubes containing sample (~2.5 mL for the 10 mm probe, ~1.0 mL for the 5 mm probe). Gas flow was interrupted using a stopped-flow system [23], followed by a delay (5–15 s) to allow the bubbles to dissipate. The temperature of the system was controlled using the variable temperature unit of the spectrometer. The Hyper-CEST experiments (5 mm probe) were conducted using a continuous wave (cw) saturation period (500 ms, applied radio frequency field strength $B_1 = 2.23$ μT), followed by a hard 90° pulse and readout of a free induction decay (50 ms). After Fourier transformation (FT) and application of an apodization filter, the xenon gas peak was referenced to 0 ppm in each spectrum for which a gas peak was present. All other spectra used the same reference for 0 ppm. Peaks were fitted to the data using the built-in fit routines in the IGOR Pro 6.1 software package (WaveMetrics Inc., Lake Oswego, OR).

Imaging experiments were conducted using a gradient coil assembly (Resonance Research Inc., Billerica, MA) for spatial encoding. Two 10 mm NMR tubes were each connected to the gas delivery system and placed side-by-side in a 30 mm NMR probe. When using two phantoms, the flow output of the polarizer was increased to 0.65 standard liters per minute. No attempt was made to compensate for differences in polarization output with increased flow. Hyper-CEST images were acquired using a cw saturation pulse (6 s, applied field strength $B_1 = 0.44$ μT) and a slice-selective 90° pulse along the z-dimension (1.2 ms, sinc shape, 13.5 mm slice-thickness) with subsequent 2-dimensional phase encoding (15×30 mm^2 field-of-view, matrix size 4×8). Each point in k-space was read out once for 1024 ms with 5 kHz spectral width. Post-processing using MATLAB® (The MathWorks Inc., Natick, MA) included two-dimensional FT for spatial reconstruction after zero-filling to an 8×16 dataset and one-dimensional FT for spectral reconstruction. Images showing the spatial distribution of the xenon signal at $\delta \approx 190$ ppm were generated by summation of the signal intensity over five data points (~0.74 ppm) in the absolute spectrum and subsequent color-encoding of these values.

Acknowledgments

Research was supported by the Director, Office of Science, Office of Basic Energy Sciences, Materials Sciences and Engineering Division and Physical Biosciences Division of the US Department of Energy under Contract No. DE-AC02-05CH11231 [TM, LS, DEW, and AP], by the Deutsche Forschungsgemeinschaft through Emmy Noether Fellowships (SCHR 995/1-1 and SCHR 995/2-1) [LS], by the European Research Council through Starting Grant Biosensor Imaging under ERC Grant Agreement No. 242710 [LS], and by a fellowship of the German Cancer Research Center [PD].

Appendix A. Supplementary material

Supplementary data associated with this article can be found, in the online version, at doi:10.1016/j.jmr.2010.05.005.

References

[1] M. Spence, S. Rubin, I. Dimitrov, E. Ruiz, D. Wemmer, A. Pines, S. Yao, F. Tian, P. Schultz, Functionalized xenon as a biosensor, Proc. Natl. Acad. Sci. 98 (2001) 10654–10657.
[2] V. Roy, T. Brotin, J.-P. Dutasta, M.-H. Charles, T. Delair, F. Mallet, G. Huber, H. Desvaux, Y. Boulard, P. Berthault, A cryptophane biosensor for the detection of specific nucleotide targets through xenon NMR spectroscopy, Chem. Phys. Chem. 8 (2007) 2082–2085.
[3] G.K. Seward, Q. Wei, I.J. Dmochowski, Peptide-mediated cellular uptake of cryptophane, Bioconjugate Chem. 19 (2008) 2129–2135.
[4] J.A. Aaron, J.M. Chambers, K.M. Jude, L. Di Costanzo, I.J. Dmochowski, D.W. Christianson, Structure of a 129Xe-cryptophane biosensor complexed with human carbonic anhydrase II, J. Am. Chem. Soc. 130 (2008) 6942–6943.
[5] C. Hilty, T.J. Lowery, D.E. Wemmer, A. Pines, Spectrally resolved magnetic resonance imaging of a xenon biosensor, Angew. Chem. Int. Ed. 45 (2006) 70–73.
[6] K. Bartik, M. Luhmer, J. Dutasta, A. Collet, J. Reisse, 129Xe and 1H NMR study of the reversible trapping of xenon by cryptophane-A in organic solution, J. Am. Chem. Soc. 120 (1998) 784–791.
[7] G. Huber, L. Beguin, H. Desvaux, T. Brotin, H. Fogarty, J.-P. Dutasta, P. Berthault, Cryptophane–xenon complexes in organic solvents observed through NMR spectroscopy, J. Phys. Chem. A 112 (2008) 11363–11372.
[8] P.A. Hill, Q. Wei, R.G. Eckenhoff, I.J. Dmochowski, Thermodynamics of xenon binding to cryptophane in water and human plasma, J. Am. Chem. Soc. 129 (2007) 9262–9263.

[9] H.E. Möller, M. Chawla, X.J. Chen, B. Driehuys, L.W. Hedlund, C.T. Wheeler, G.A. Johnson, Magnetic resonance angiography with hyperpolarized 129Xe dissolved in a lipid emulsion, Magn. Reson. Med. 41 (1999) 1058–1064.
[10] G. Duhamel, P. Choquet, E. Grillon, L. Lamalle, J.-L. Leviel, A. Ziegler, A. Constantinesco, Xenon-129 MR imaging and spectroscopy of rat brain using arterial delivery of hyperpolarized xenon in a lipid emulsion, Magn. Reson. Med. 46 (2001) 208–212.
[11] R. Smith, E. Porter, K. Miller, The solubility of anesthetic gases in lipid bilayers, Biochim. Biophys. Acta 645 (1981) 327–338.
[12] A. Venkatesh, L. Zhao, D. Balamore, F. Jolesz, M. Albert, Evaluation of carrier agents for hyperpolarized xenon MRI, NMR Biomed. 13 (2000) 245–252.
[13] M. Spence, E. Ruiz, S. Rubin, T. Lowery, Development of a functionalized xenon biosensor, J. Am. Chem. Soc. 126 (2004) 15267–15294.
[14] G. Huber, T. Brotin, L. Dubois, H. Desvaux, J.-P. Dutasta, P. Berthault, Water soluble cryptophanes showing unprecedented affinity for xenon: candidates as NMR-based biosensors, J. Am. Chem. Soc. 128 (2006) 6239–6246.
[15] S. Rubin, M. Spence, I. Dimitrov, E.J. Ruiz, A. Pines, D.E. Wemmer, Detection of a conformational change in maltose binding protein by 129Xe NMR spectroscopy, J. Am. Chem. Soc. 123 (2001) 8616–8617.
[16] A. Cherubini, A. Bifone, Hyperpolarised xenon in biology, Prog. Nucl. Magn. Reson. Spectrosc. 42 (2003) 1–30.
[17] L. Schröder, T. Meldrum, M. Smith, T. Lowery, D.E. Wemmer, A. Pines, Temperature response of 129Xe depolarization transfer and its application for ultra-sensitive NMR detection, Phys. Rev. Lett. 100 (2008) 257603(4).
[18] L. Schröder, T. Lowery, C. Hilty, D. Wemmer, A. Pines, Molecular imaging using a targeted magnetic resonance hyperpolarized biosensor, Science 314 (2006) 446–449.
[19] K. Ruppert, J. Brookeman, K. Hagspiel, J. Mugler III, Probing lung physiology with xenon polarization transfer contrast (XTC), Magn. Reson. Med. 44 (2000) 349–357.
[20] VS Bajaj, T. Meldrum, D.E. Wemmer, A. Pines, Application of multiple-pulse saturation transfer sequences to hyperpolarized 129Xe, J. Magn. Reson., submitted for publication.
[21] W. Happer, E. Miron, S. Schaefer, D. Schreiber, W. Van Wijngaarden, X. Zeng, Polarization of the nuclear spins of noble-gas atoms by spin exchange with optically pumped alkali-metal atoms, Phys. Rev. A 29 (1984) 3092–3110.
[22] T. Walker, W. Happer, Spin-exchange optical pumping of noble-gas nuclei, Rev. Mod. Phys. 69 (1997) 629–642.
[23] S.-I. Han, S. Garcia, T.J. Lowery, E.J. Ruiz, J.A. Seeley, L. Chavez, D.S. King, D.E. Wemmer, A. Pines, NMR-based biosensing with optimized delivery of polarized 129Xe to solutions, Anal. Chem. 77 (2005) 4008–4012.